# Internal Impedance in Determining Usability of Used Lithium-Ion Batteries in Second-Life Applications

Minh Tran, Jussi Sihvo, and Tomi Roinila

***Abstract*—Li-ion batteries have become key energy storage devices in powering various industrial processes and consumer products. Increased demand for Li-ion batteries has raised environmental issues because most of the batteries are landfilled upon reaching end of life. However, studies have suggested that most of the used Li-ion batteries can be reused in second-life applications. Battery state parameters such as the state-of-health (SOH) and state-of-charge (SOC) are typically used for assessing the performance. The SOH is particularly useful in predicting the remaining life cycle of the battery and selecting suitable second-life applications for reuse. However, measuring the SOH can be difficult using existing technology. Recent studies have shown that a battery's internal impedance can be used to determine the SOH of the battery. This paper demonstrates the applicability of the internal impedance in evaluating the SOH and suitability of used Li-ion batteries in second-life applications. Experimental measurements from several commercial Li-ion batteries are shown and analyzed. The work is a revised and extended version of a presentation at ECCE2022 [1].**

***Index Terms*—Ageing, correlation analysis, electrochemical impedance spectroscopy, fourier methods, Li-ion batteries, second life.**

## I. Introduction

LI-ION batteries have become key energy storage devices in powering electric vehicles, consumer electronics, and various industrial products. The wide applicability of Li-ion batteries is attributed to the battery high-performance properties such as high energy density and high power density [2]. The global Li-ion battery market size is projected to reach approximately 100 billion euros by 2030 [3]. As a result, development of the recycling processes for Li-ion batteries plays an important role to the sustainable future of the technology. Efficient battery recycling have significant effects to many areas including the supply chain of raw manufacturing materials and reducing the environmental impact of battery waste [4].

Despite the increasing production of Li-ion batteries, battery recycling is currently limited [5]. Approximately 95 percent of all Li-ion batteries are landfilled instead of recycled upon reaching end of life. Landfilled batteries may catch fire or produce hydrogen fluoride formation if the electrolyte is exposed to water. Such environmental impacts prevent a sustainable future for Li-ion batteries. However, studies suggest that almost 95 percent of the battery waste could be recycled as raw material recycling or as battery reuse in second-life applications [6]. Second-life reuse of Li-ion batteries applies particularly to electric vehicle waste batteries. The performance of battery storage in electric vehicles is usually considered unsuitable when the storage capacity degrades to less than 80 percent of the original capacity [7]. Second-life battery capacity produced by electric vehicles is estimated to hit over 275 GWh per year, which presents huge opportunities for different energy storages [8], [9], [10]. One example would be to reuse the capacity as grid-level storage devices. Although sophisticated technologies exist for extracting and recycling usable minerals from used cells, there are currently no feasible methods for determining cells that are still usable.

In second-life applications, the remaining storage capacity of a battery is an important performance indicator, which is typically indicated by the battery state-of-health (SOH). The SOH indicates the storage capacity of the battery in reference to the nominal capacity and can be used to study the battery suitability to a second-life application [11], [12]. In practice, however, obtaining the SOH directly is challenging [13].

Studies have shown that useful information about the battery state-of-health (SOH) can be obtained using the battery's internal impedance [14], [15], [16], [17], [18], [19], [20]. A conventional method for obtaining the impedance is to apply electrochemical impedance spectroscopy (EIS) in which sinusoidal perturbations are injected on top of the battery nominal output current to produce output voltage responses. The resulting battery voltage and current are measured and analyzed using Fourier methods to obtain the battery impedance at various frequencies. While the EIS produces an accurate measurement of the impedance, the method is limited to laboratory environment due to impractical and costly implementation; this is due to the construction of sinusoidal waves requiring many signal levels and each single sinusoidal wave contains energy for only a single frequency.

Recent studies have proposed broadband methods, such as the pseudo-random binary sequence (PRBS), to measure batteries' internal impedance [21], [22], [23]. The PRBS is a broadband signal that contains energy at several frequencies in a single period. Therefore, applying PRBS excitation to measure the

Manuscript received 2 February 2023; revised 6 April 2023; accepted 8 May 2023. Date of publication 29 May 2023; date of current version 20 September 2023. Paper 2023-TSC-0025.R1, presented at the 2022 IEEE Energy Conversion Congress and Exposition, Detroit, MI, USA, Oct. 09–13, and approved for publication in the IEEE Transactions on Industry Applications by the Transportation Systems Committee of the IEEE Industry Applications Society [DOI: 10.1109/ECCE50734.2022.9947891]. *(Corresponding author: Minh Tran.)*

The authors are with the Department of Electrical Engineering, Tampere University, 33100 Tampere, Finland (e-mail: minh.tran@tuni.fi; jussi.sihvo@tuni.fi; tomi.roinila@tuni.fi).

Color versions of one or more figures in this article are available at https://doi.org/10.1109/TIA.2023.3280466.

Digital Object Identifier 10.1109/TIA.2023.3280466

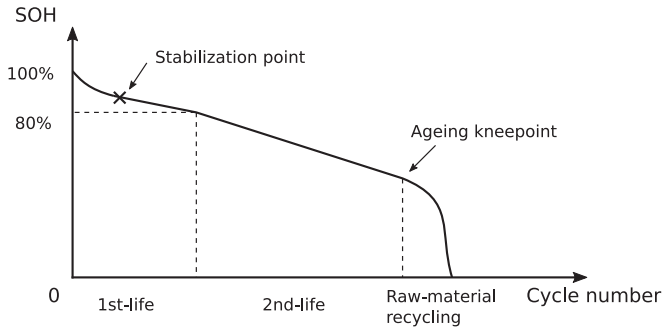


Fig. 1. SOH curve of a Li-ion cell life cycle.

impedance can be done in a fraction of the time required in traditional EIS applications. In addition, as the PRBS is in a binary form, the excitation is very easy to generate in practice using a low-cost signal generator, the output of which can only deal with a small number of signal levels [24].

This paper demonstrates the applicability of using the internal impedance in evaluating used Li-ion batteries performance for second-life applications. Several commercial Li-ion batteries were tested in the experiments. Simple statistical analysis was applied to examine the relationship between the impedance and second-life performance of the batteries.

The remainder of the paper is organized as follows. Section II provides theoretical basis for the ageing mechanisms of the battery and how they are related to the lifecycle. Section III presents the methods for battery impedance measurement and analysis. Section IV presents experimental measurements based on several commercial Li-ion battery cells. Finally, Section V draws conclusions.

## II. Theory

The life cycle of a Li-ion battery can be divided into several stages: mining of raw materials, battery manufacturing, first-life application, second-life application and the raw-material extraction at the recycling factory. Raw-material extraction can then be succeeded by battery manufacturing to form a circular economy. Fig. 1 conceptually demonstrates a part of the full life cycle of a Li-ion battery cell, during which the cell operates as an electrical energy storage device, in terms of cycle number and the SOH. The SOH is typically expressed as a percentage of the maximum storage capacity at the time of the measurement out of the rated capacity [25]. Typical examples of first-life applications can be found in electric vehicles. The first life of a battery spans from the first cycle until the capacity loss reaches more than the 20 percent limit that is conventionally used by the automotive industry [7]. After the first life, the cell is disposed of for recycling or reused in second life. Second-life applications can include energy storages for grid-connected photovoltaic power systems. As the SOH reaches the aging knee point, charge capacity drops rapidly and the cell is considered unusable [12], [26]. The second-life viability of a Li-ion battery cell can be evaluated based on the amount of charge the cell can supply before reaching the aging kneepoint.

Li-ion battery degradation is characterized by the loss of energy storage capacity and power capability over time. The level of degradation is typically described by measurable parameters such as charge-capacity fading and increase of the battery cell internal resistance [25], [27], [28], [29]. Loss of capacity and increased internal resistance are caused by various naturally-occuring aging processes such as corrosions of electrode materials, increasing thickness of the solid-electrolyte interface (SEI) layer, electrolyte depletion [29], [30], [31]. External factors such as high load current, high temperature, overvoltage and over-discharge accelerate the speed of the aging processes, which leads to a shorter lifetime.

The most dominant aging mechanism in a Li-ion battery cell is the growth of the solid-electrolyte interface (SEI) layer, which takes place at the surface of the negative electrode [29], [32], [33]. As the cell charges and discharges many cycles over time, the thickness and coverage of the SEI layer increase by consuming both the negative electrode and the electrolyte material as a result of various reduction processes [34], [35]. Although the SEI layer serves as a stabilizing substance for the cell which ensures a long-term performance by reducing electrolyte decomposition, it consumes the lithium ions inventory as it grows, resulting in a loss of charge capacity of the cell. Increased SEI thickness also results in higher inhibition of ionic flow, and thus higher internal resistance over time. Besides the composition of the negative-electrode and the electrolyte material, the formation of SEI layers also depends on external factors such as temperature and concentration of electrolyte salt [35].

The main degradation mechanism at the end of the usable lifetime of a Li-ion battery is the formation of lithium dendrite, or lithium plating [36]. Lithium dendrites are formed on the surface of the SEI layers due to the uneven distribution of ionic flow and ionic concentration in the electrolyte and in the electrodes. The lithium plating process is magnified at high charge/discharge current and at low temperature [29]. When the dendrite is long enough, it reaches through the separator and short-circuits the two electrodes with electronic flow. The short circuit results in a thermal runaway, which is highly dangerous as the fire is self-sustainable.

As Fig. 1 demonstrates, the cell SOH experiences an initial rapid drop in the beginning due to the increasing consumption of lithium ions by the SEI layer [27]. The speed of capacity fading then reduces and stabilizes as the cycle life continues. The decreased speed of capacity fading is related to the stabilization of the SEI layer, which inhibits further decomposition of the electrolyte material, resulting in a fairly linear drop of capacity as the cycle number progresses [32], [33]. Other factors including corrosion of the electrodes and electrolyte decomposition also takes part in the capacity fading during the usable lifecycle of the battery. As the lifecycle progresses, the SOH reaches the aging kneepoint, where the maximum charge capacity suffers a sudden rapid drop [37], [38]. At this point, the rate of capacity fading changes from linear to nonlinear and the aging knee is typically associated with excessive formation of lithium dendrite beyond a stable limit. Identification of the aging knee provides a termination condition for second-life operations of a Li-ion battery cell.

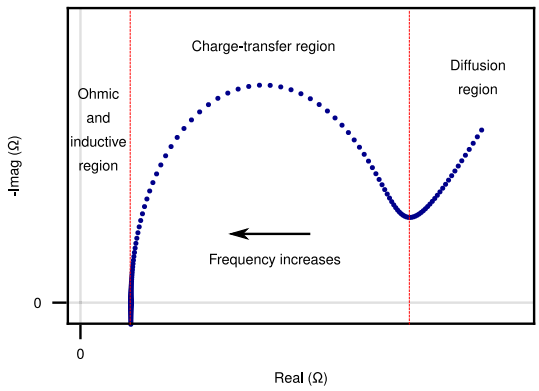


Fig. 2. Nyquist plot of a Li-ion battery impedance.

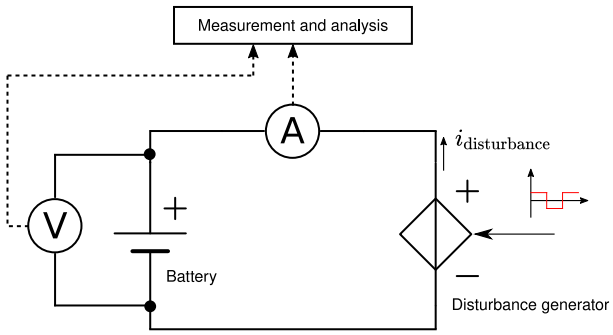


Fig. 3. Conceptual battery impedance measurement setup.

## III. Methods

Studies have shown the use of the battery cell internal impedance as a convenient SOH indicator [14], [15], [16], [17], [18], [19], [20]. The internal impedance gives direct information of the dynamic states inside a battery cell, based on which useful state parameters can be derived. Fig. 2 shows a typical impedance spectrum of a Li-ion battery in a Nyquist plot. The imaginary axis is usually inverted so that the capacitive characteristic of the impedance is shown in the first quadrant of the complex plane. Several regions of the impedance curve can be defined based on the frequency ranges, where each describes a different set of physical phenomena in the battery. Starting from the right-hand side of the diagram, low-frequency diffusion processes in the electrodes, typically less than a few hundred mHz, are represented by a 45° rising line. In the middle range of frequency, which ranges from a few hundred mHz to a few kHz, semicircular arches are formed by the dynamics of the SEI layer and the charge transfering in the electrolyte. At higher frequencies, ohmic and inductive behavior dominates and describes the overall dynamics of the battery.

### A. Measuring the Impedance

The basic principle for measuring the battery cell internal impedance is demonstrated in Fig. 3. An external current disturbance is applied to charge and discharge the battery based on an excitation waveform to produce a voltage response at the battery terminals. The excitation can be designed to excite the battery at a range of frequencies. The resulting battery current and output voltage are measured, and Fourier transform is applied to the measured signals to obtain the spectral information of the impedance.

The battery's internal impedance is conventionally measured by applying electrochemical impedance spectroscopy (EIS) [39]. In the method, the battery is perturbed by sinusoidal waves of current at various frequencies as demonstrated in Fig. 3, and the impedance is obtained in the frequency domain using Fourier methods. However, the EIS is difficult to implement in practice due to the signal construction of sinusoidal waves requiring many signal levels. Another limitation is that single-frequency injection based on sinusoidal waves takes a long time to measure for the whole impedance bandwidth.

Recent studies have demonstrated broadband methods based on pseudo-random binary sequence (PRBS) perturbations to measure the battery impedance in real-time [21], [22], [23], [40]. In the methods, the battery under test is charged and discharged according to the PRBS excitation as demonstrated in Fig. 3. The voltage and current responses are measured and Fourier transform is applied to obtain the impedance in the frequency domain. Measuring the impedance using the PRBS significantly reduces the measurement time compared to the conventional EIS as the signal carries spectral energy at several frequencies in a single period. In addition, because the PRBS is in binary form, the excitation can be easily injected to the battery current [24].

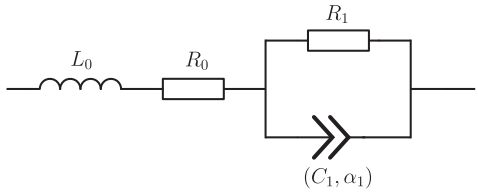


Fig. 4. Randles battery impedance equivalent circuit model.

### B. Equivalent Circuit Modeling

Equivalent circuit modeling is a popular and practical approach in the dynamical analysis and control of Li-ion batteries [19], [41], [42]. An equivalent circuit model (ECM) can accurately approximate the dynamics of a battery while requiring inexpensive computational resources [16], [43]. The experimental method applied in this paper utilizes a circuit model as shown in Fig. 4, based on the Randles ECM popularly used for modeling chemical batteries [44].

The circuit in Fig. 4 consists of an equivalent series inductor ($L_0$), an equivalent series DC resistor ($R_0$), and a parallel resistor-nonlinear-capacitor group ($R_1$ and $(C_1, \alpha_1)$) which represents the mid-frequency range charge-transfer processes. The capacitor component $(C_1, \alpha_1)$ in the circuit is a non-linear component called the constant-phase element (CPE) that approximates the double-layer capacitance of the solid-electrolyte layers [45]. The impedance of the CPE as a function of frequency

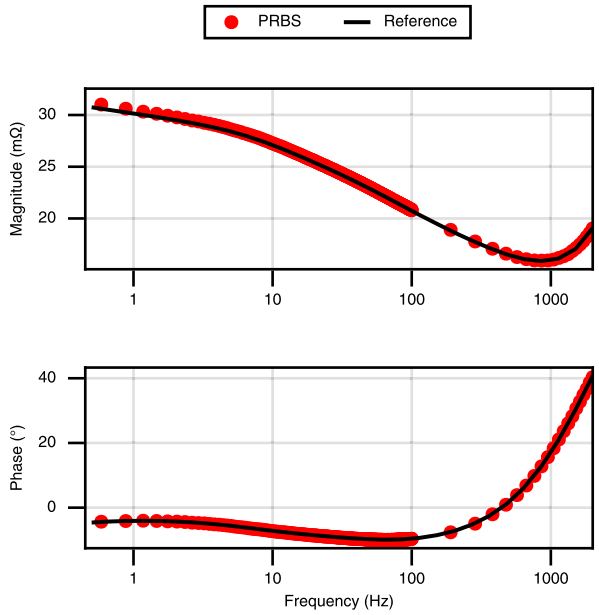


Fig. 5. Impedance measurements of a Li-ion battery cell using EIS and PRBS.

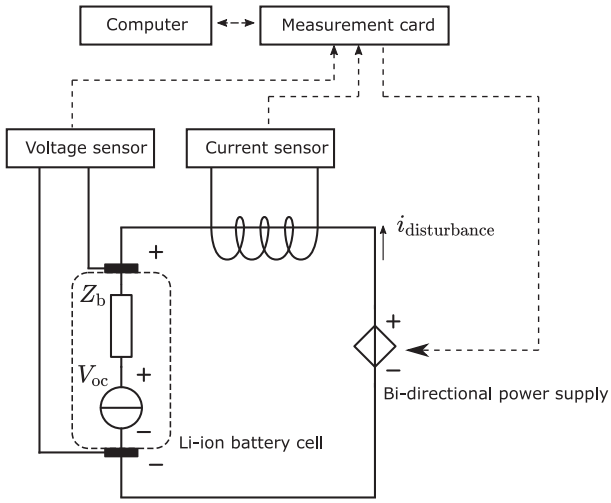


Fig. 6. Impedance measurement setup.

$\omega$ is given as

$$Z_{\text{CPE}}(\omega) = \frac{1}{(j\omega)^{\alpha_1} C_1} \tag{1}$$

where $\alpha_1$ $(0 < \alpha_1 \leq 1)$ is called the suppression factor of the semi-circular arch formed by the parallel $R_1$ and CPE. The ECM parameters are often empirically estimated by fitting the non-parametric impedance measurement of the battery to the circuit model using nonlinear complex least-square method [46].

## IV. Experiments

### A. Verification of PRBS-Measurement Method

The first experiment was conducted to verify the applied PRBS-measurement technique. Fig. 6 depicts the measurement setup used to obtain the battery cell impedance. In the measurement, a current excitation is injected into a battery cell (LG-HE2-18650) by the bi-directional power supply according to the designed waveform. Both the PRBS and the conventional EIS-method were applied to measure the impedance. The PRBS excitation amplitude was selected as 0.5 A and the generation frequency was selected as 6 kHz. The measurement using PRBS was done in two separate sub-measurements. The first measurement covered the bandwidth from 0.5 Hz to 100 Hz and the second measurement covered the bandwidth from 100 Hz to 2 kHz. The cell voltage and input current were measured by the measurement card. The Fourier transform was then applied to the measured voltage and current to obtain the spectral data of the internal impedance.

Fig. 5 shows the impedance measurement using both the PRBS and the EIS (reference). As the figure shows, the impedance obtained by the PRBS accurately follows the reference in a wide range of frequencies.

### B. Second-Life Emulation Experiment

Several experimental measurements were carried out to demonstrate the effectiveness of the battery internal impedance in evaluating the battery SOH. A set of 12 used battery cells were collected at a recycling plant that has been used in a first-life application. The model of the cells is LG ICR18650 MF1 which is a rechargeable cylindrical Li-ion battery cell type with lithium-cobalt-oxide (LCO) as the positive-electrode material and graphite as the negative-electrode material, a polymer-based porous membrane as the electronic separator and a composition of lithium salts dissolved in organic solvents as the electrolyte [47]. The cells are designed for light-weight electric vehicle applications, presumably retrieved from a battery pack of an electric scooter or bicycle. The cells have 2150 mAh nominal charge capacity and 1.075 A standard charge current. The previous history in the first-life application of the cells is unknown.

*1) Impedance Measurement:* The internal impedance of each battery cell was measured in the beginning of the experiment at room temperature (22 °C). The PRBS excitation was used in the experiment using the same parameters as in the first experiment. Fig. 7 shows the measured impedance of the cells in a Nyquist plot.

*2) Accelerated Aging:* Accelerated aging process was applied to all the battery cells at room temperature (22 °C) using repeated full charge/discharge cycling. For each charge/discharge cycle, constant-voltage-constant-current (CV-CC) charging method at the full-charge voltage of 4.2 V, charge current of 1.75 A (0.8 C) and the termination current of 50 mA was applied to charge the cell from 0 percent SOC to 100 percent SOC. During the discharge, constant-current (CC) discharge method at the discharge current of 1.75 A (0.8 C) and the cut-off voltage of 2.75 V was applied to discharge the cell from 100 percent SOC to 0 percent SOC. Before each charge-cycle, the cells rested at zero percent SOC for 30 minutes in order to stabilize their temperature and thermodynamic states. Maximum charge-capacity value was recorded for each cell at every cycle which is then used

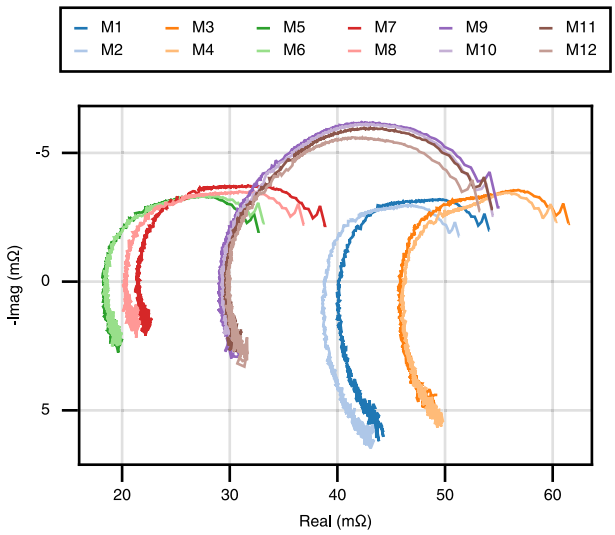


Fig. 7. Impedance measurements of used Li-ion battery cells.

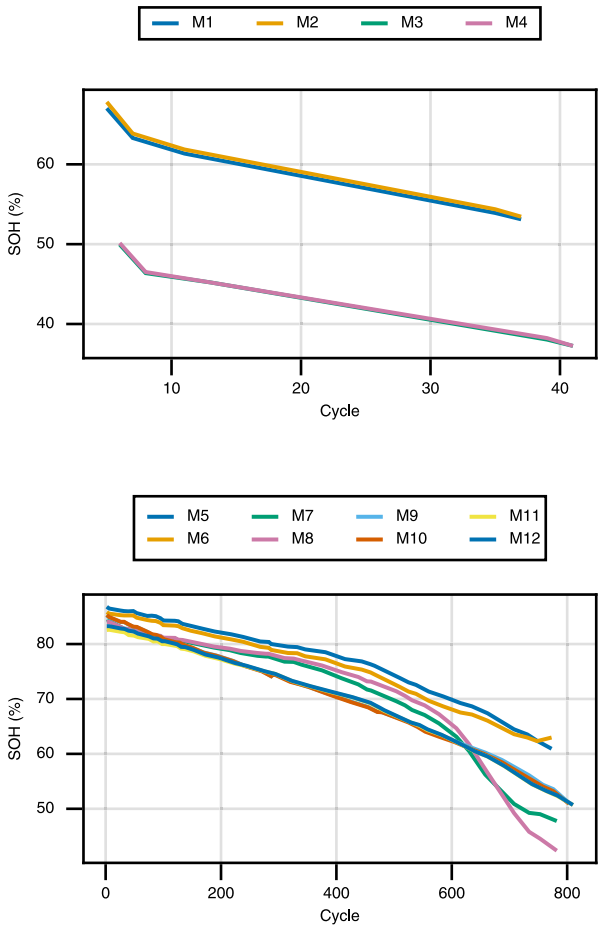


Fig. 8. State-of-health (capacity fading) of the cells during the cycling.

for computing the state-of-health (SOH) by calculating the ratio of the measured capacity and the nominal capacity (2150 mAh). The cells were cycled up to 800 cycles. Fig. 8 shows the SOH for each cell as a function of cycle number. The cycling of cells M1 to M4 stopped as early as 40 cycles due to exceptionally rapid loss of capacity and were categorized as low-quality cells. For the other cells in the experiment, the SOH values remained above 70 percent up to 600 cycles. Cells M7 and M8 started to reach the aging kneepoint, as reflected by a suddenly rapid loss of SOH as early as 600 cycles, while the other cells showed relatively linear capacity fading, indicating longer usable life.

### C. Correlation Analysis

The experimental results from Figs. 7 and 8 can be combined to draw conclusions about the relationship between the cell internal impedance values and the cells aging behavior. An equivalent circuit model (ECM) as depicted in Fig. 4 was applied to model the battery dynamics. A non-linear least-squared fitting method for complex number was applied using MATLAB Optimization Toolbox to fit the measured impedance data to the circuit model parameters: $L_0$, $R_0$, $R_1$, $C_1$ and $\alpha_1$. The fit is then plotted against the impedance measurement data for verification. Fig. 9 shows the plot of the measured impedance and the ECM fit for cells M2 and M10 as an example.

A correlation analysis was applied to give insights into the relationships between the internal impedance and the aging of the batteries. The correlation coefficient is a parameter that indicates the level of a linear association between two random variables expressed as

$$r = \frac{\mathrm{cov}(X, Y)}{\sigma_X \sigma_Y} \tag{2}$$

where $r$ is the coefficient, $\mathrm{cov}(X, Y)$ is the covariance of the random variables $X$ and $Y$, and $\sigma_X$, $\sigma_Y$ are the standard deviations of $X$ and $Y$, respectively. The correlation coefficient value is always between -1 and 1, in which the closer absolute value of the coefficient is to 1 the higher chance that the variables are linearly associated to each other. Similarly, the closer the coefficient value is to zero the more likely it is that the variables are independent and unrelated to each other. A positive correlation coefficient indicates that, when mapped together, the variables tends to simultaneously increase or decrease with each other and a negative coefficient indicates that the variables tends to move in opposite directions with each other.

The certainty of a correlation coefficient is typically evaluated using the standard error of correlation coefficient given as

$$\sigma_r = \sqrt{\frac{1 - r^2}{n - 2}} \tag{3}$$

where $\sigma_r$ is the standard error and $n$ is the sample size. A smaller standard error indicates a more confident linear correlation as described by the coefficient.

Three parameters obtained from the capacity measurement result were used to characterize the aging effect of the battery: the SOH at the end of the cycling ($\mathrm{SOH}_{\mathrm{final}}$), the overall loss of SOH over the whole cycling period ($\Delta$SOH), and the average speed of loss of SOH ($\frac{\Delta \mathrm{SOH}}{\Delta \mathrm{cycle}}$) defined as the average SOH loss

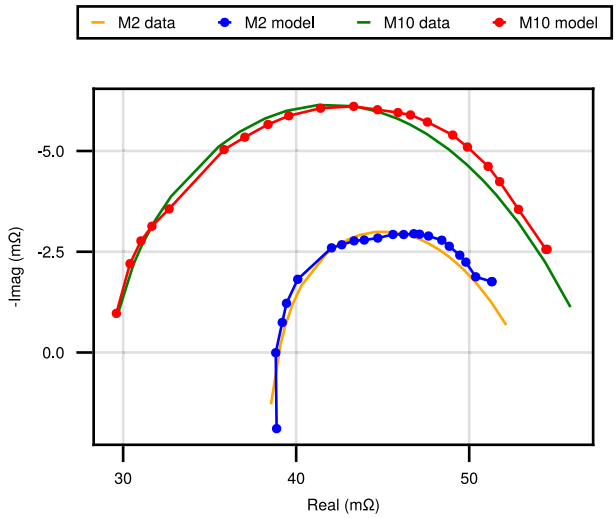


Fig. 9. Impedance curves of the impedance measurement data and the equivalent circuit models of cells M2 and M10 at selected frequency harmonics.

per cycle

$$\frac{\Delta \text{SOH}}{\Delta \text{cycle}} = \frac{\text{SOH}_{\text{initial}} - \text{SOH}_{\text{final}}}{\text{Total number of cycles}} \tag{4}$$

The final SOH values for each cell were taken from the capacity measurement of the last cycle, except for cells M7 and M8 where the last SOH values were taken at the 600th cycle.

The ECM parameters were correlated against the SOH-related parameters by computing the correlation coefficients to examine the linear relationships between the impedance parameters and the SOH. The open-source Julia computing environment and its libraries were used in the calculation of the correlation coefficients. The standard errors of the coefficients were also obtained using the same platform. In addition to computing the coefficients for all the cells, the analysis was applied to smaller subsets of the whole dataset based on the observation that some cells have very similar DC resistance values (crossing points on the horizontal axis in the Nyquist diagram located closely to each other). In particular, subset S1 consists of cells M1 to M4, subset S2 consists of cells M5 to M8 and subset S3 contains cells M9 to M12. The following subsets were also defined to increase the confidence of the correlation analysis result: S12, which contains cells M1 to M8; S23, which contains cells M5 to M12; and S13, which contains cells M1 to M4 and M8 to M12. The whole dataset is denoted as S.

Table I shows the correlation coefficients of the ECM parameters against the SOH-based parameters (with standard errors shown in the parentheses) where only the relationships with all-positive or all-negative coefficients across the subsets S, S12, S23, and S13 are shown. The table indicates that the internal DC resistance $R_0$ shows very high correlation to both the final storage capacity (SOH) and the average speed of capacity fading (speed of SOH loss). Fig. 10 visualizes the relationships between the internal DC resistance and the SOH with a linear regression for each plot.

TABLE I
CORRELATION COEFFICIENTS OF EQUIVALENT CIRCUIT PARAMETERS AND AGING PARAMETERS FROM MULTIPLE SUB-DATASETS

| Correlation | S12 | S23 | S13 | S |
|---|---|---|---|---|
| $L_0 \parallel \text{SOH}_{\text{final}}$ | -0.7 (0.3) | -0.26 (0.4) | -0.15 (0.4) | -0.53 (0.3) |
| $R_0 \parallel \text{SOH}_{\text{final}}$ | -0.92 (0.2) | -0.69 (0.3) | -0.97 (0.1) | -0.89 (0.2) |
| $L_0 \parallel \frac{\Delta \text{SOH}}{\Delta \text{cycle}}$ | 0.95 (0.1) | 0.94 (0.1) | 0.24 (0.4) | 0.95 (0.1) |
| $R_0 \parallel \frac{\Delta \text{SOH}}{\Delta \text{cycle}}$ | 0.95 (0.1) | 0.9 (0.2) | 0.95 (0.1) | 0.86 (0.2) |
| $C_1 \parallel \Delta \text{SOH}$ | 0.11 (0.4) | 0.88 (0.2) | 0.98 (0.1) | 0.79 (0.3) |
| $\alpha_1 \parallel \Delta \text{SOH}$ | -0.08 (0.4) | -0.95 (0.1) | -0.76 (0.3) | -0.82 (0.2) |

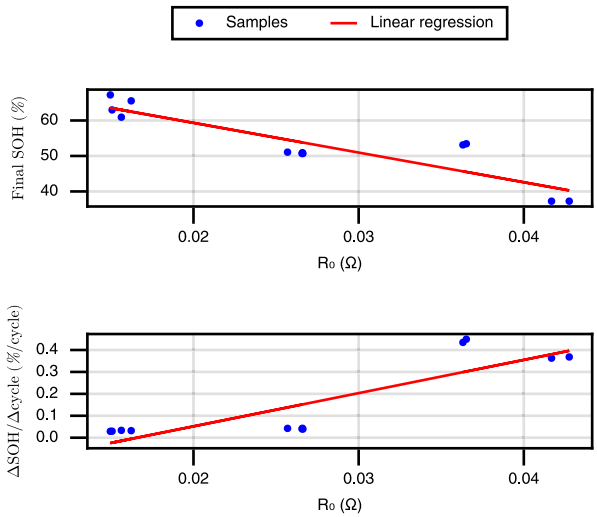


Fig. 10. Linear regressions of mappings between DC resistance $R_0$ and aging parameters.

TABLE II
CORRELATION COEFFICIENTS OF EQUIVALENT CIRCUIT PARAMETERS AND AGING PARAMETERS FROM SUB-DATASETS WITH SIMILAR DC RESISTANCE VALUES

| Correlation | S1 | S2 | S3 |
|---|---|---|---|
| $L_0 \parallel \text{SOH}_{\text{final}}$ | 0.52 (0.6) | 0.39 (0.7) | 0.26 (0.7) |
| $R_0 \parallel \text{SOH}_{\text{final}}$ | -0.99 (0.1) | -0.11 (0.7) | -0.8 (0.4) |
| $\alpha_1 \parallel \text{SOH}_{\text{final}}$ | -0.71 (0.5) | -0.51 (0.6) | -0.56 (0.6) |
| $C_1 \parallel \frac{\Delta \text{SOH}}{\Delta \text{cycle}}$ | 0.86 (0.4) | 0.82 (0.4) | 0.47 (0.6) |
| $\alpha_1 \parallel \frac{\Delta \text{SOH}}{\Delta \text{cycle}}$ | -0.67 (0.5) | -0.35 (0.7) | -0.69 (0.5) |
| $C_1 \parallel \Delta \text{SOH}$ | 0.91 (0.3) | 0.94 (0.2) | 0.46 (0.6) |

Table II shows the correlation coefficients of the ECM parameters against the SOH-based parameters where only all-positive or all-negative correlations across the subsets S1, S2, and S3 are shown (with standard errors shown in the parentheses). It can be seen from the table that, for cells of similar DC resistance values, the charge-transfer capacitance $C_1$ may potentially be used to indicate the speed of capacity fading due to the consistently high correlations across the datasets.

TABLE III
INTERNAL RESISTANCE AND CHARGE-TRANSFER CAPACITANCE ECM PARAMETERS OF CELLS M5 → M12

| | M5 | M6 | M7 | M8 | M9 | M10 | M11 | M12 |
|---|---|---|---|---|---|---|---|---|
| $R_0$(mΩ) | 15.6 | 15.1 | 16.2 | 15.0 | 25.7 | 26.6 | 26.6 | 26.6 |
| $C_1$(F) | 0.42 | 0.39 | 0.38 | 0.35 | 0.47 | 0.49 | 0.47 | 0.47 |
| $R_1$(mΩ) | 19.4 | 21.1 | 25.5 | 25.4 | 32.4 | 30.5 | 30.7 | 29.5 |

TABLE IV
INTERNAL RESISTANCE AND CHARGE-TRANSFER CAPACITANCE ECM PARAMETERS OF CELLS M1 → M4

| | M1 | M2 | M3 | M4 |
|---|---|---|---|---|
| $R_0$ (mΩ) | 36.3 | 36.5 | 41.7 | 42.7 |
| $C_1$ (F) | 0.4 | 0.45 | 0.38 | 0.38 |
| $R_1$ (mΩ) | 20.3 | 16.5 | 23.0 | 20.9 |

### D. Analysis of Degradation Processes

The degradation processes can be analyzed by using the experimental results. As shown in Fig. 8, cells M1 to M4 (low-quality cells) showed very rapid loss of charge capacity and were discarded early on in the cycling experiment. However, the SOH of these cells dropped linearly with the cycle number. A similar observation was made for cells M9 to M12. The capacity fading curves of these cells were linear, which indicates that the dominant degradation process has been the consumption of lithium-ions due to the growth of the SEI layer [32], [33]. On the other hand, the capacity loss of cells M5 to M8 showed as nonlinear and less predictable curves, which implied less dominant effects by the (thinner) SEI layers. As a result, other degradation processes including electrode corrosions and electrolyte depletion had more significant effects to the aging of such cells. Nevertheless, the thinner SEI layers resulted in cells M5 to M8 retaining more charge capacity (higher cycling efficiency) than the other cells during the cycling process. By the end of the experiment, the SOH curves of cells M5, M6 and M9 to M12 have the potential to extend by several hundreds of additional cycles into the future. Cells M7 and M8, however, experienced the aging knees around the 600th cycle. The aging knees of these cells indicate that lithium plating became the dominant aging process after the occurrences of the kneepoints.

The results of the correlation analysis has provided information from which the initial cell impedance spectra can be linked to the occurred aging processes. Table III shows the relevant ECM parameters of cells M5 to M12 (high-quality cells) based on the results of the correlation analysis. The charge-transfer resistance ($R_1$) was also included to show the relations between the SEI layer thickness and the aging of the cells. It can be seen that group S2 (cells M5 to M8) have lower values for all the parameters compared to group S3 (cells M9 to M12). The thinner SEI layers of group S2 are reflected in smaller charge-transfer capacitance ($C_1$) and smaller charge-transfer resistance ($R_1$). Within group S2, cells M7 and M8 have smaller charge-transfer capacitance ($C_1$) but higher charge-transfer resistance ($R_1$) than M5 and M6 which indicates a thicker but a lower level of porosity in the SEI particles. A relatively high-thickness with low-porosity SEI layer indicates a low-kinetic charge-transfer process, which is a precondition to lithium plating. It was also observed that cells M7 and M8 has the lowest values of charge-transfer capacitance ($C_1$) compared to all other cells in the whole dataset. The differences in SEI layer degradation of cells within a battery pack might be due to uneven thermal distribution, which led to different SEI formation temperatures [34].

Considering group S1 (cells M1 to M4), it is clear from Fig. 7 that they have the highest internal resistance (located farther into the right-hand side of the complex plane) and performed the worst. However, the charge-transfer capacitance ($C_1$) and resistance ($R_1$) of these cells have similar magnitude to group S2 but with slightly less resistance as shown in Table IV. This could imply that while the speed of degradation for group S1 is fast, their SEI layer remains sufficiently stable and could be utilized in a low-power second-life application.

### E. Cell Sorting Procedure

Battery energy storage applications are typically classified based on the energy and power capability requirements. Based on the analysis and experimental results, a systematic method for sorting of used cells based on their impedance characteristics for suitable second-life applications is proposed as follows.

1) Measure the battery cell impedance
2) Formulate the ECM and obtain the ECM parameters from the impedance measurement
3) Classify potential applications based on the impedance characteristics:

- Low internal resistance → High-power applications
- High internal resistance → Low-power applications
- Low charge-transfer resistance and capacitance → High-energy long-term storage applications
- High charge-transfer capacitance → Long-term storage applications
- High charge-transfer resistance and low charge-transfer capacitance → High-energy applications

The proposed procedure is a qualitative method based on the experimental results using the given dataset. However, in practice, the sorting protocol applied should use well-defined threshold values to sort the cells into the suitable applications with more complex requirements. The practical sorting protocol should be developed based on a much larger experimental dataset.

### F. Discussion and Future Work

The experiment has shown that some parameters of the impedance ECM such as the DC resistance $R_0$ and charge-transfer capacitance $C_1$ can be used to give predictive information of the battery cells capability to operate in a second-life application. However, the experimental work has certain limitations as follows. The information of first-life operation of the test cells were unknown when the experimental work was carried out. Such information could provide useful information about the cell performance. While the initial impedance measurement was measured and used in the analysis, the evolution of battery impedance as the battery cycling proceeds may also play a critical role in determining the future SOH. For example, it was not straight-forward based only on the initial impedance

measurements to apply predictive analysis to determine the approaching knees of cells M7 and M8. The size of the dataset (12 battery cells) is very small which affects the confidence of the statistical inference analysis. Finally, while the opinionated selection of ECM parameters in the analysis has given satisfactory results, it may not be suitable in practice and is still subjected to fitting optimization errors. Such limitations from the experimental work will be addressed in the future work on the topic.

## V. Conclusion

This paper has demonstrated the use of the battery internal impedance measurement in efficiently evaluating the battery SOH in a second-life application. Experimental measurements of commercial battery cells impedance were applied using broadband methods and accelerated aging. Experimental results and analysis have shown correlation between the internal impedance and second-life storage capabilities of Li-ion battery cells. The applied method can be used, for example, to rapidly measure a large number of end-of-life battery cells and to define their applicability for second-life applications. The future work will include more experimental studies for a larger number and different types of battery cells.

## References


[1] M. Tran, T. Messo, R. Luhtala, J. Sihvo, and T. Roinila, "Used lithium-ion batteries in second-life applications: Feasibility study," in *Proc. IEEE Energy Convers. Congr. Expo.*, 2022, pp. 1–5.

[2] G. Zubi, R. Dufo-López, M. Carvalho, and G. Pasaoglu, "The lithium-ion battery: State of the art and future perspectives," *Renewable Sustain. Energy Rev.*, vol. 89, pp. 292–308, 2018.

[3] M. E. Market, "Growth, trends, COVID-19 impact, and forecasts (2021–2026)," Research and Markets (report), Tech. Rep. 4515727, Apr. 2021.

[4] J. Li, Y. Lu, T. Yang, D. Ge, D. L. Wood III, and Z. Li, "Water-based electrode manufacturing and direct recycling of lithium-ion battery electrodes–A green and sustainable manufacturing system," *IScience*, vol. 23, no. 5, 2020, Art. no. 101081.

[5] J. Heelan et al., "Current and prospective li-ion battery recycling and recovery processes," *JOM*, vol. 68, no. 10, pp. 2632–2638, 2016.

[6] S. King and N. J. Boxall, "Lithium battery recycling in Australia: Defining the status and identifying opportunities for the development of a new industry," *J. Cleaner Prod.*, vol. 215, pp. 1279–1287, 2019.

[7] A. Sonoc, J. Jeswiet, and V. K. Soo, "Opportunities to improve recycling of automotive lithium ion batteries," *Procedia CIRP*, vol. 29, pp. 752–757, 2015.

[8] "Second-life electric vehicle batteries 2020–2030," IDTechEx, Tokyo, Japan, Tech. Rep. 187, 2020.

[9] L. C. Casals, B. A. García, and C. Canal, "Second life batteries lifespan: Rest of useful life and environmental analysis," *J. Environ. Manage.*, vol. 232, pp. 354–363, 2019.

[10] E. Hossain, D. Murtaugh, J. Mody, H. M. R. Faruque, M. S. H. Sunny, and N. Mohammad, "A comprehensive review on second-life batteries: Current state, manufacturing considerations, applications, impacts, barriers & potential solutions, business strategies, and policies," *IEEE Access*, vol. 7, pp. 73215–73252, 2019.

[11] M. H. S. M. Haram, J. W. Lee, G. Ramasamy, E. E. Ngu, S. P. Thiagarajah, and Y. H. Lee, "Feasibility of utilising second life EV batteries: Applications, lifespan, economics, environmental impact, assessment, and challenges," *Alexandria Eng. J.*, vol. 60, no. 5, pp. 4517–4536, 2021.

[12] E. Martinez-Laserna et al., "Technical viability of battery second life: A study from the ageing perspective," *IEEE Trans. Ind. Appl.*, vol. 54, no. 3, pp. 2703–2713, May/Jun. 2018.

[13] C. Lin, A. Tang, and W. Wang, "A review of SOH estimation methods in lithium-ion batteries for electric vehicle applications," *Energy Procedia*, vol. 75, pp. 1920–1925, 2015.

[14] X. Wang et al., "A review of modeling, acquisition, and application of lithium-ion battery impedance for onboard battery management," *eTransportation*, vol. 7, pp. 1–21, 2021.

[15] X. Wang, X. Wei, H. Dai, and Q. Wu, "State estimation of lithium ion battery based on electrochemical impedance spectroscopy with on-board impedance measurement system," in *Proc. IEEE Veh. Power Propulsion Conf.*, 2015, pp. 1–5.

[16] D. N. How, M. Hannan, M. H. Lipu, and P. J. Ker, "State of charge estimation for lithium-ion batteries using model-based and data-driven methods: A review," *IEEE Access*, vol. 7, pp. 136116–136136, 2019.

[17] U. Tröltzsch, O. Kanoun, and H.-R. Tränkler, "Characterizing aging effects of lithium ion batteries by impedance spectroscopy," *Electrochimica Acta*, vol. 51, no. 8/9, pp. 1664–1672, 2006.

[18] D. I. Stroe, M. Swierczynski, A. I. Stan, V. Knap, R. Teodorescu, and S. J. Andreasen, "Diagnosis of lithium-ion batteries state-of-health based on electrochemical impedance spectroscopy technique," in *Proc. IEEE Energy Convers. Congr. Expo.*, 2014, pp. 4576–4582.

[19] T. Kim et al., "An on-board model-based condition monitoring for lithium-ion batteries," *IEEE Trans. Ind. Appl.*, vol. 55, no. 2, pp. 1835–1843, Mar./Apr. 2019.

[20] E. Locorotondo et al., "Impedance spectroscopy characterization of lithium batteries with different ages in second life application," in *Proc. IEEE Int. Conf. Environ. Elect. Eng., IEEE Ind. Commercial Power Syst. Eur.*, 2020, pp. 1–6.

[21] J. Sihvo, D.-I. Stroe, T. Messo, and T. Roinila, "Fast approach for battery impedance identification using pseudo-random sequence signals," *IEEE Trans. Power Electron.*, vol. 35, no. 3, pp. 2548–2557, Mar. 2020.

[22] E. Locorotondo et al., "Electrochemical impedance spectroscopy of li-ion battery on-board the electric vehicles based on fast nonparametric identification method," in *Proc. IEEE Int. Conf. Environ. Elect. Eng., IEEE Ind. Commercial Power Syst. Eur.*, 2019, pp. 1–6.

[23] A. Fairweather, M. Foster, and D. Stone, "Battery parameter identification with pseudo random binary sequence excitation (PRBS)," *J. Power Sources*, vol. 196, no. 22, pp. 9398–9406, 2011.

[24] K. Godfrey, "Introduction to binary signals used in system identification," in *Proc. Int. Conf. Control*, 1991, pp. 161–166.

[25] M. Broussely et al., "Main aging mechanisms in Li-ion batteries," *J. Power Sources*, vol. 146, no. 1/2, pp. 90–96, 2005.

[26] E. Martinez-Laserna et al., "Evaluation of lithium-ion battery second life performance and degradation," in *Proc. IEEE Energy Convers. Congr. Expo.*, 2016, pp. 1–7.

[27] J. Vetter et al., "Ageing mechanisms in lithium-ion batteries," *J. Power Sources*, vol. 147, no. 1/2, pp. 269–281, 2005.

[28] C. R. Birkl, M. R. Roberts, E. McTurk, P. G. Bruce, and D. A. Howey, "Degradation diagnostics for lithium ion cells," *J. Power Sources*, vol. 341, pp. 373–386, 2017.

[29] A. Barré, B. Deguilhem, S. Grolleau, M. Gérard, F. Suard, and D. Riu, "A review on lithium-ion battery ageing mechanisms and estimations for automotive applications," *J. Power Sources*, vol. 241, pp. 680–689, 2013.

[30] S. J. An et al., "Correlation of electrolyte volume and electrochemical performance in lithium-ion pouch cells with graphite anodes and NMC532 cathodes," *J. Electrochem. Soc.*, vol. 164, no. 6, 2017, Art. no. A1195.

[31] S. J. An et al., "Electrolyte volume effects on electrochemical performance and solid electrolyte interphase in Si-Graphite/NMC lithium-ion pouch cells," *ACS Appl. Mater. Interfaces*, vol. 9, no. 22, pp. 18799–18808, 2017.

[32] J. Wang et al., "Degradation of lithium ion batteries employing graphite negatives and nickel-cobalt-manganese oxide spinel manganese oxide positives: Part 1, aging mechanisms and life estimation," *J. Power Sources*, vol. 269, pp. 937–948, 2014.

[33] M. Ecker et al., "Calendar and cycle life study of li (NiMnCo) $O_2$-based 18650 lithium-ion batteries," *J. Power Sources*, vol. 248, pp. 839–851, 2014.

[34] V. A. Agubra and J. W. Fergus, "The formation and stability of the solid electrolyte interface on the graphite anode," *J. Power Sources*, vol. 268, pp. 153–162, 2014.

[35] S. J. An, J. Li, C. Daniel, D. Mohanty, S. Nagpure, and D. L. Wood III, "The state of understanding of the lithium-ion-battery graphite solid electrolyte interphase (SEI) and its relationship to formation cycling," *Carbon*, vol. 105, pp. 52–76, 2016.

[36] T. Waldmann, B.-I. Hogg, and M. Wohlfahrt-Mehrens, "Li plating as unwanted side reaction in commercial li-ion cells–A review," *J. Power Sources*, vol. 384, pp. 107–124, 2018.

[37] T. C. Bach et al., "Nonlinear aging of cylindrical lithium-ion cells linked to heterogeneous compression," *J. Energy Storage*, vol. 5, pp. 212–223, 2016.

[38] E. Braco, I. San Martín, A. Berrueta, P. Sanchis, and A. Ursúa, "Experimental assessment of cycling ageing of lithium-ion second-life batteries from electric vehicles," *J. Energy Storage*, vol. 32, 2020, Art. no. 101695.
[39] D. D. Macdonald, "Reflections on the history of electrochemical impedance spectroscopy," *Electrochimica Acta*, vol. 51, no. 8/9, pp. 1376–1388, 2006.
[40] M. Tran, T. Roinila, and J. Markkula, "Realtime internal-impedance measurement of lithium-ion battery using discrete-interval-binary-sequence injection," in *Proc. IEEE Energy Convers. Congr. Expo.*, 2022, pp. 1–5.
[41] M. Hossain, S. Saha, M. T. Arif, A. M. Oo, N. Mendis, and M. E. Haque, "A parameter extraction method for the li-ion batteries with wide-range temperature compensation," *IEEE Trans. Ind. Appl.*, vol. 56, no. 5, pp. 5625–5636, Sep./Oct. 2020.
[42] R. Zhao, P. J. Kollmeyer, R. D. Lorenz, and T. M. Jahns, "A compact methodology via a recurrent neural network for accurate equivalent circuit type modeling of lithium-ion batteries," *IEEE Trans. Ind. Appl.*, vol. 55, no. 2, pp. 1922–1931, Mar./Apr. 2019.
[43] C. Zhang, W. Allafi, Q. Dinh, P. Ascencio, and J. Marco, "Online estimation of battery equivalent circuit model parameters and state of charge using decoupled least squares technique," *Energy*, vol. 142, pp. 678–688, 2018.
[44] J. E. B. Randles, "Kinetics of rapid electrode reactions," *Discuss. Faraday Soc.*, vol. 1, pp. 11–19, 1947.
[45] G. Brug, A. L. van den Eeden, M. Sluyters-Rehbach, and J. H. Sluyters, "The analysis of electrode impedances complicated by the presence of a constant phase element," *J. Electroanalytical Chem. Interfacial Electrochemistry*, vol. 176, no. 1/2, pp. 275–295, 1984.
[46] J. R. Macdonald, J. Schoonman, and A. Lehnen, "Applicability and power of complex nonlinear least squares for the analysis of impedance and admittance data," *J. Electroanalytical Chem. Interfacial Electrochemistry*, vol. 131, pp. 77–95, 1982.
[47] Q. Li, J. Chen, L. Fan, X. Kong, and Y. Lu, "Progress in electrolytes for rechargeable li-based batteries and beyond," *Green Energy Environ.*, vol. 1, no. 1, pp. 18–42, 2016.